# Supporting Information

Labro et al. 2018

## SI Material and Methods

**Materials:** Superdex HR 200 column was purchased from GE. Cobalt resin for protein purification was purchased from Thermofisher. LB media, mammalian cell growth media and other reagents (ampicillin, Isopropyl β-D-1-thiogalactopyranoside and glucose) were purchased from Difco or Sigma. Dodecyl maltoside, Decyl maltoside and Triton X-100 were purchased from Anatrace. PEG-400, crystallization reagents, crystallization plates were purchased from Hampton Research. The antibody used for crystallization was a gift from R. Mackinnon (Rockefeller University). Spin label (1-oxyl-2,2,5,5- tetramethyl-D3-pyrroline-3-methyl methanethiosulfonate) was obtained from Toronto Research Chemicals. Asolectin polar extract was purchased from Avanti. Chemical reagents and buffers were purchased from Sigma-Aldrich. QuickChange Kit II was purchased from Agilent.

**Molecular Biology:** KcsA cloned in pQE-70 (C-terminus His-tagged), human Kv1.5 cloned in pBK-CMV and the N-terminal deletion mutant Δ6–46 *Shaker* channel cloned in pGW1 vectors were mutated (the 2$^{nd}$ threonine within the signature sequence of $K^+$ dchannels -TTVGYGD- was substituted with an alanine) by using the QuickChange site-directed mutagenesis kit (Stratagene, La Jolla, CA, USA). After PCR based mutagenesis, double-strand sequencing of the entire constructs confirmed the presence of the desired modification and the absence of unwanted mutations.

**Electrophysiology for eukaryotic channels:** The human Kv1.5 cloned in the pBK-CMV vector was expressed in a mammalian $Ltk^-$ cell line (mouse fibroblast cells, ATCC number CCL-1.3). Electrophysiological recordings for *Shaker*-IR and Shaker-IR-T442A (IR=fast inactivation removed (1)) were obtained from expression in HEK293 cells since the Shaker construct expresses poorly in Ltk- cells. $Ltk^-$ cells were grown on culture dishes (6 cm in diameter) using Dulbecco´s Modified Eagle Medium (DMEM) supplemented with 10% horse serum and 1% penicillin/streptomycin (Invitrogen, Carlsbad, CA, USA). HEK293 cells were cultured in Modified Eagle´s Medium (MEM) supplemented with 10% fetal bovine serum, 1% penicillin/streptomycin and 1% non-essential amino acids

(Invitrogen, Carlsbad, CA, USA). Cells (60% confluent dishes) were transiently transfected with appropriate concentrations of plasmid DNA (ranging from 0.5 to 5 µg) using polyethyleneimine (2) that was purchased from Sigma-Aldrich (ST Luis, MO, USA). Approximately 20 to 48 hours (for Kv1.5-T480A, Kv3.1-T400A, and *Shaker*-T442A) after transfection, cells were harvested by trypsinization and transferred to a recording chamber mounted on the stage of an inverted microscope. Whole-cell ionic current measurements were done at room temperature (20 to 23°C) with an Axopatch-200B amplifier and the recordings were digitized with a Digidata-1200A (Molecular Devices, Sunnyvale, CA, USA). Command voltages and data storage were controlled with pClamp10 software. Patch pipettes were pulled from 1.2 mm quick-fill borosilicate glass capillaries (World Precision Instruments) with a P-2000 puller (Sutter Instrument Co., Novato, CA, USA) and afterwards heat polished using a micro-forge. For the non-stationary noise experiments, the tip of the patch pipettes was coated with sylgard® 184silicon elastomer (Dow Corning, Midland, MI, USA). During current measurements, the cells were constantly superfused with an external bath solution that in standard conditions contained (in mM) NaCl 130, KCl 4, $CaCl_2$ 1.8, $MgCl_2$ 1, HEPES 10, Glucose 10, adjusted to pH 7.35 with NaOH. External solutions with elevated $K^+$ concentration or 10 mM $Rb^+$, used to study the speed of selectivity-filter conversion from its inactivated and collapsed state to its conducting open conformation as a function of external $K^+$ or $Rb^+$ concentration, were obtained by replacing NaCl with KCl. Different external bath solutions were applied to the cells with a custom build pressurized fast switching perfusion system (valves were purchased from the Lee Company, Westbrook, CT, USA) and a quartz micromanifold (ALA scientific, Farmingdale, NY, USA), allowing rapid exchange of the external bath solutions. The patch pipettes were filled with an internal solution containing (in mM) KCl 110, $K_4$BAPTA 5, $K_2$ATP 5, $MgCl_2$ 1, NaCl 1, HEPES 10, and adjusted to pH 7.2 with KOH. The junction potentials were zeroed with the filled pipette in the bath solution and experiments were excluded from analysis if the voltage error estimate exceeded 5 mV after series resistance compensation.

Data Analysis: Details of pulse protocols used to elicit ionic currents were adjusted to determine the biophysical properties of each construct adequately and are shown in the figures or described in legends. The conductance vs. voltage (GV) curve of both channel

activation and inactivation was in all cases fitted with a Boltzmann distribution: $y = 1/\{1 + \exp[-(V - V_{1/2})/k]\}$, where $V$ represents the applied voltage, $V_{1/2}$ the midpoint potential at which 50% of the channels have opened or inactivated, and $k$ the slope factor. The kinetics of the ionic currents were determined by fitting the rise in current activation ($I_{ac}$) or decay during deactivation ($I_{deac}$) with a single or double exponential function.

The single channel conductance of the WT channels and the alanine for threonine substitution variants were estimated with non-stationary noise analysis. Activating ionic currents were recorded in the whole-cell configuration and the applied pulse protocol consisted of 100 repetitive depolarizations to +40 mV. Channels composed of the alanine for threonine substitution were recruited in their conducting configuration with repetitive depolarizations before applying the pulse protocol used for non-stationary noise analysis. For both WT and mutant channels, only cells that did not display current rundown during the train of repetitive depolarizations were used for analysis. Current recordings were analyzed using the built-in non-stationary fluctuation analysis tool of Pclamp10 software. This analysis tool calculates the ensemble current variance ($\sigma^2$) of the 100 tracings and plot it as a function of total current. This relation was then approximated with the parabolic function $\sigma^2 = iI - i^2/n$, where i is the single channel current, I the total current, and n the number of channels. Subsequently, the single channel conductance was calculated from the obtained single channel current i.

**KcsA expression and purification:** KcsA T75A in the closed(3) or the locked-open scaffold (with KcsA activation locked-open by disulfide bonds(4)) were transformed into *E. coli*-XL10-Gold cells and grown overnight at $37^0$C in LB media supplemented with 1% glucose and 0.4 mg/ml ampicillin(5). Next day, the overnight culture was diluted 100 times into 1 L of Luria-Bertani (LB) broth supplemented with 0.5% glycerol, 0.2 % glucose and 0.4 mg/ml ampicillin at $37^0$C. When cells reached an optical density at 600 nm (O.D) of 0.6, the cultures were cooled down to $29^0$C for 1 hour. Next, 0.1 mM isopropyl thiogalactoside (IPTG), 10 mM $BaCl_2$ (a $K^+$ channel blocker) and 0.4 mM ampicillin were added and cells were incubated for 24 hours at constant agitation (250 rpm) at $29^0$C. Next day, the cells were harvested at 4600 rpm and expression levels were quantified by western blot. Cells were resuspended in a buffer (Buffer A: 50 mM Tris-HCl: 150 mM KCl) supplemented with + 170 ug/ml phenylmethylsulfonyl fluoride and treated with 0.5 mg/mL

of egg lysozyme by rotation at room temperature for 1 h. The cell suspension was passed through a microfluidizer and then spun down at 100,000 g for 1 h to pellet the cell membranes. The membrane preparation was resuspended with Buffer A containing protease inhibitors, and aliquots were stored at -80 °C. KcsA was extracted from the *E. coli* membrane by solubilizing it with Buffer A + 20 mM DDM + protease inhibitors for 1 h at room temperature. The solubilized protein was separated from the insoluble material by spinning down at 100,000 g. The supernatant was loaded onto a cobalt resin column and washed with Buffer A supplemented with 10 mM imidazole and 1 mM DDM and eluted it with Buffer A supplemented with 1 mM DDM and 400 mM imidazole. The analysis of KcsA properly-folded was performed by size-exclusion chromatography on an ENrich SEC 650 10x300 column (Bio-Rad).

**KcsA electrophysiology:** T75A mutant or KcsA wild-type channels were reconstituted in Asolectin liposomes(6). Channels were reconstituted at a 1 to 20-100 protein-to-lipid ratio (weight/weight), to be able to measure macroscopic currents, in Asolectin liposomes that were made with the following buffer: 200 mM KCl and 5 mM MOPS-buffer at pH 7.0 (Buffer B). KcsA containing liposomes were incubated overnight with bio-beads SM-2 from Bio-Rad. After 24 hours incubation time, proteoliposomes suspension was harvested by centrifugation at 100,000 g for 1 hour. The KcsA-containing liposomes pellet was resuspended in 60 μL of buffer B. Three drops of this proteoliposomes suspension were placed on a microscope glass slide and dehydrated overnight in a desiccation chamber. After 24 hours, the three dried drops were rehydrated with 20 μl of Buffer B at 4°C overnight. Normally, the samples were rehydrated for ~24 hours, which yielded giant liposomes appropriate for patch-clamp measurements. KcsA electrophysiology was performed in symmetrical 5 mM MOPS at the desired pH in the presence of 200 mM KCl. KcsA currents were recorded by several independent experiments (n=10 to 3 repeats) with a patch-clamp amplifier Axopatch 200 B, and currents were sampled at 40 kHz with an analogue filter set to 10 kHz. Patch pipettes, after fire polishing, displayed a resistance of 2.0 MΩ (they were filled with 200 mM KCl and 5 mM MOPS-buffer at pH 4.0). Macroscopic currents for the wild-type channel and the T75A mutant were baseline corrected and digitally filtered on Campfit (Axon Instrument) amplitude normalized in Origin 9 (OriginLab) to compare the kinetic of C-type inactivation. Chord conductance and

NPo for the wild-type and T75A channels were determined from Gaussian fitting to closed and open events distributions in all point histogram.

**Continuous wave electron paramagnetic resonance spectroscopy (CW-EPRs) measurements:** ~2.5 mg of purified KcsA-T75A-G116C was concentrated to 10 mg/ml, cysteines were kept reduced by adding 1 mM tris(2-carboxyethyl)phosphine (TCEP). A desalting column, PD-10 (GE Healthcare), previously equilibrated with an oxygen depleted buffer at pH 7 (buffer with no detergent was bubbled with nitrogen gas for 30 minutes to decrease the partial pressure of molecular oxygen), was used to clean the excess of TCEP. KcsA-T75A-G116C at 10 mg/ml was incubated with a 10-fold molar excess of the spin-label (SL) (1-oxyl-2,2,5,5-tetramethyl-Δ3-pyrroline-3-methyl methanethiosulfonate) (Toronto Research) for 30 min on ice. Since the half-life of the spin label in aqueous solution is 1 hour (it is highly reactive with itself), a second pulse of SL was added and allowed to react for 1 hour. The sample was cleaned from the of SL by passing it through a size exclusion chromatography column, ENrich SEC 650 10x300 (Bio-Rad). Lastly, spin labeled-channels were reconstituted into preformed polar extract lipid liposomes at 1:1600 (KcsA-tetramer:lipid) molar ratio, by the dilution method followed by an addition of bio-beads for 2 hours (Bio-Rad) to remove the detergent. After two hours, KcsA-containing liposomes were harvested by centrifugation at 100,000 g.
KcsA's activation: Liposomes were resuspended at pH 7 and divided in 6 tubes (the channel is closed at neutral pH) and harvested by a centrifugation at 100,000 g. Next, the pH was gradually decreased by resuspending each pellet in a high-capacity buffer with different pHs (100 mM citrate-phosphate, 150 mM KCl), followed by a centrifugation step at 100,000 g. Next, Samples were study by CW-EPRs to determine the energetics of KcsA activation gating, i.e., the closed→open transition. Then CW-EPR pH-dependent spectra were acquired. KcsA's deactivation: as before the liposome pellet was resuspended and equilibrated in a high-capacity buffer but this time at pH 3, (at pH 3 KcsA is fully activated) followed by a centrifugation step at 100,000 g to collect the proteoliposomes. KcsA's deactivation gating was measured by increasing gradually the pH and measuring the consequent set of CW-EPR spectra. 5 µl of sample were loaded in a sealed quartz capillary and CW-EPR spectra were recorded using a dielectric

resonator (ER 4123D), with 2 mW incident power, 100 kHz modulation frequency and 1 G field modulation amplitude. KcsA's activation and deactivation pKas were determined from the half-maximal effective concentration of $[H^+]$ of the normalized amplitude of the central resonance line of the CW-EPR spectra vs $[H^+]$ curves, by fitting a Hill Equation.

**KcsA crystallography:** Chymotrypsin-cut KcsA (T75A-closed or T75A-locked open scaffold) was complexed with an antibody fragment used for crystallization purposes and purified it by passing it through a size exclusion chromatography column ENrich SEC 650 10x300 column (Bio-Rad) pre-equilibrated with Buffer A + 5 mM Decyl Maltoside. Crystal trials were set up by sitting-drop method in 24-27 % PEG400 (v/v), 50 mM magnesium acetate, 50 mM sodium acetate (pH 5.4-6.0) at 19 °C. Crystals regularly appeared within a two-weeks period and they were immediately cryo-protected by increasing the concentration of PEG-400 to 40% by 5% increment per day. Frozen crystals diffracted to Bragg spacing of 2.35 Å, the T75A-closed structure and 2.37 Å, T75A-open structure. Crystallographic data were collected at the beamline 14-1 at the Stanford Synchrotron Radiation Laboratory (SSRL) from a single crystal. Image processing and data reduction were performed with HKL2000(7).

**Crystallographic Analysis**. The crystallographic structures of the KcsA-T75A-closed (PDB=6BY2) and the KcsA-T75A-open (PDB=6BY3) conformations were solved by molecular replacement. The coordinates of the antibody fragment from the original KcsA structure at 2 Å resolution (PDB-1K4C)(8) was used as the search model. The structural models for the closed and open conformation of the T75A mutant were built from scratch using coot(9) and refined iteratively with Phenix(10), including rigid body, energy minimization, simulated annealing and individual B-factor refinements. The crystallographic data analysis statistics are reported in the Table 1. The figures on this paper were made using Pymol ( https://pymol.org )

## Table 1

| | GV curve | | selectivity | | g(pS) | |
|---|---|---|---|---|---|---|
| | $V_{1/2}$ (mV) | slope k | ratio $Na^+/K^+$ | *n* | | *n* |
| *WT* ***Kv1.5*** | -14.3 ± 1.0 | 5.8 ± 0.2 | 0.010 ± 0.002 | 8 | 12.6 ± 1.5 | 5 |
| *T480A* | -20.7 ± 1.1 | 5.7 ± 0.2 | 0.010 ± 0.002 | 5 | 5.7 ± 0.7 | 3 |
| ***Shaker*** | -20.3 ± 2.3 | 6.4 ± 1.2 | 0.011 ± 0.003 | 4 | 15.0 ± 3.4 | 3 |
| *T442A* | -42.2 ± 2.0 | 5.8 ± 0.6 | 0.010 ± 0.001 | 6 | 6.0 ± 0.4 | 3 |

Permeability ration Na/K determined from the $E_{rev}$ potential (I = 0nA) obtained using deactivation pulse protocols (Figure S3). Ratio $Na^+/K^+$ was calculated using the GHK equation and solutions: external 4mM K / 150mM Na, internal 145mM K/ 0.5mM Na.

**Table 2**

| Statistic | T75A-closed | T75A-open |
|---|---|---|
| **Space Group** | I4 | I4 |
| Cell Dimension | | |
| *a=b, c (Å)* | 157.17, 75.45 | 156.12, 74.47 |
| *α=β=Y (°)* | 90 | 90 |
| Resolution (Å) | 27.22 -2.35 (2.43- | 34.91-2.37 (2.45 -2.37) |
| $R_{merge}$ | 0.153 (0.44) | 0.076 (0.59) |
| I/σI | 7.67 (2.64) | 18.62 (2.0) |
| Completeness (%) | 99.12 (99.71) | 99.37 (97.97) |
| Redundancy | 3.7 (3.6) | 3.9 (4.0) |
| **Refinement** | | |
| No. reflections | 38148 (3805) | 36365 (3571) |
| $R_{work}$ | 0.22 (0.28) | 0.20 (0.25) |
| $R_{free}$ | 0.24 (0.33) | 0.22 (0.26) |
| No. atoms | 4168 | 4112 |
| Protein | 4003 | 3941 |
| Ligand/ion | 3 | 6 |
| Waters | 121 | 124 |
| Other ligands | 44 | 47 |
| Protein residues | 534 | 528 |
| Bond lengths (Å) | 0.003 | 0.003 |
| Bond angles (°) | 0.59 | 0.58 |
| Wilson B-factor | 50.67 | 48.63 |
| Average B-Factor, $Å^2$ | 59.88 | 58.41 |
| Protein | 59.87 | 58.46 |
| Ligands | 73.49 | 64.62 |
| Water | 55.24 | 54.35 |
| Ramachandran | 96.78 | 97.12 |
| Ramachandran | 0.19 | 0.00 |

*Highest resolution shell is show in parenthesis.

** Data sets were collected from a single crystal.

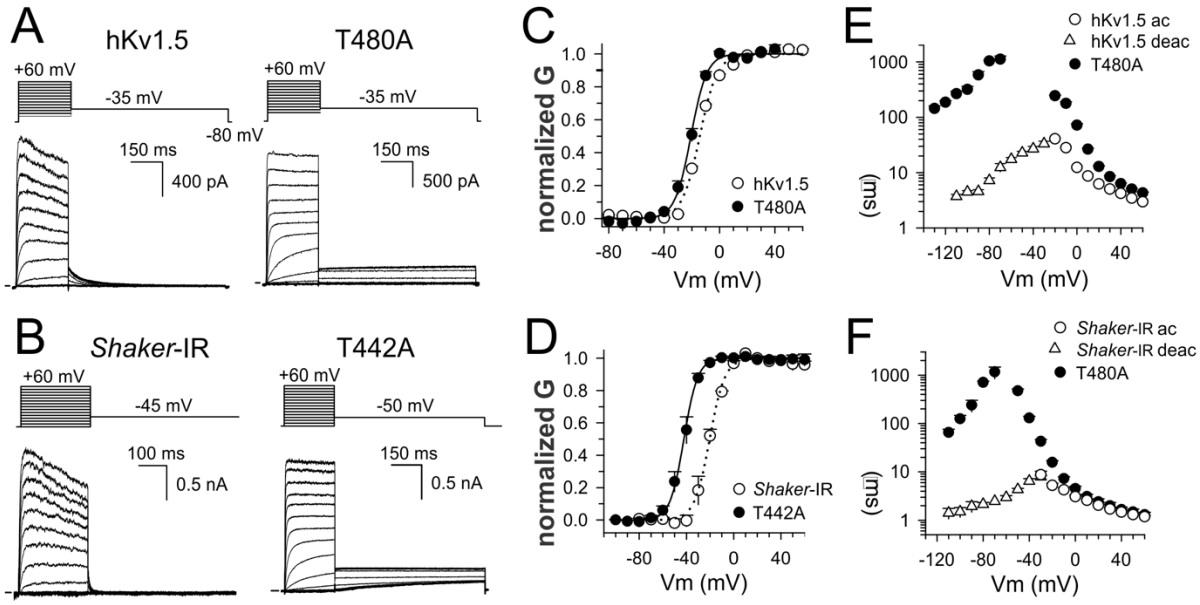


**Fig. S1.** 2nd-T-to-A mutations produced voltage gated $K^+$ channels. Representative macroscopic current recordings for the wild-type channels and their corresponding 2nd-T-to-A mutations, hKv1.5 (**a.**) and *Shaker* (**b.**). Current recordings were elicited with the pulse protocols shown on top and the zero-current level is indicated by the horizontal bar at the start of the recordings. After applying activating depolarizing pulses, the cell membrane potential was stepped back to a fixed value that deactivates the channel and elicit the corresponding tail currents (e.g. -35 mV in the case of hKv1.5 and its T480A mutant). In Panel **c** and **d**, are shown the voltage dependence of channel activation for the hKv1.5 and the channels channels (open circles) and their T-to-A mutations (filled circles). The conductance (G) versus voltage (V) relationship or GV curves were obtained by plotting the normalized conduction G (obtained by normalizing the tail current amplitudes from pulse protocols shown in panel **a.** and **b.)** as a function of the voltage changes. Compared to WT channels the T-to-A mutations shifted slightly the GV curve towards more hyperpolarized potentials. Data are average values ± standard-error of the mean (SEM), with solid and dotted line representing the average fit with a Boltzmann function (GV curves midpoint and slope factor are reported in table 1). Panels **e** and **f** display the activation (open circles) and deactivation (triangles) time constants for the

wild-type channels, hKv1.5 (**e**) and *Shaker* (**f**). Activation time constants were obtained by fitting the activation phase of the macroscopic currents shown in panels **a** and **b** with a single exponential function (note the semi-logarithmic axis). The deactivation time constants were obtained from analyzing the current decay upon different repolarizing potentials (pulse protocols are shown in supplemental figure 3). The activation and deactivation time constants of the T-to-A mutants were obtained in a similar manner and are displayed with filled circles in panels **e**. and **f**. (values represent mean ± se from 3 to 8 independent observations).

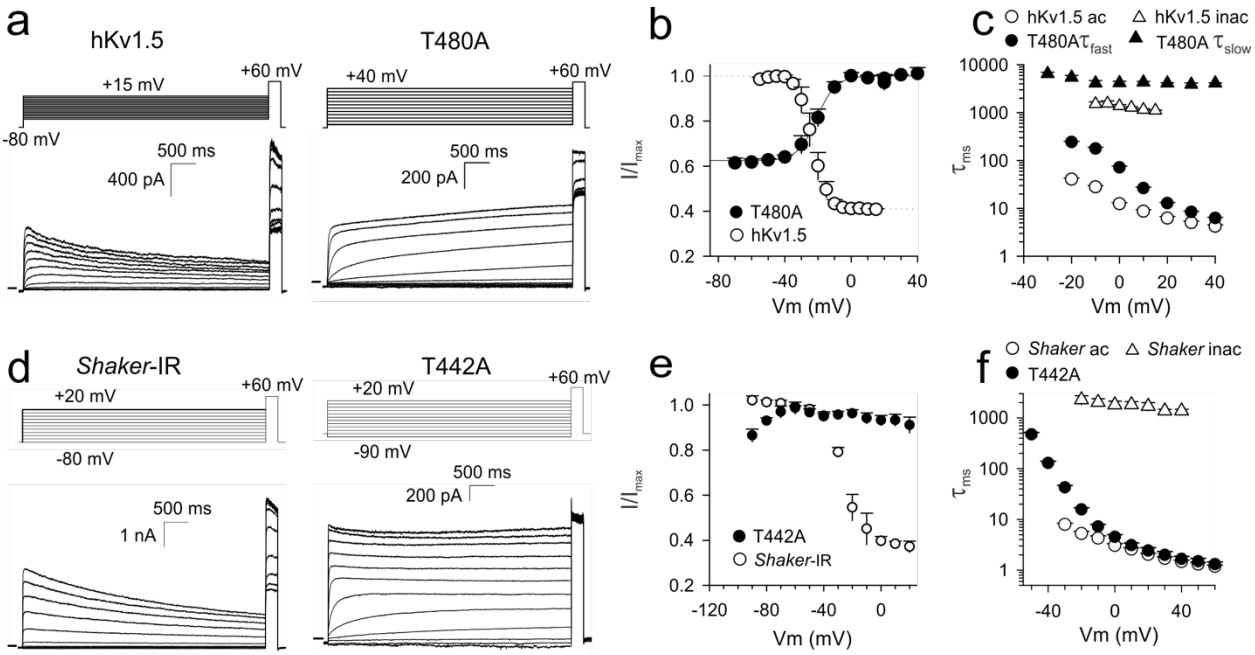


**Fig. S2.** Inactivation kinetics of the hKv1.5, Shaker and their 2nd-T-to-A mutant channels. Panels **a** and **b** show representative macroscopic current recordings for hKv1.5 (**a**) and Shaker (**d**) channels (wild-type and 2nd-T-to-A mutations). Current recordings were elicited with the pulse protocols shown on top and the zero-current level is indicated by the horizontal bar at the start of the recordings. Prolonged depolarizations induce inactivation in wild-type channels resulting in a gradual decrease in current amplitude. The degree of channel inactivation after 5s depolarization was determined by applying an activating test pulse to +60 mV, which elicited a macroscopic current amplitude that reports directly on the number of channels that did not inactivate. In contrast to the wild-type channel, the 2nd-T-to-A mutants did not display the gradual decrease in current amplitude upon prolonged depolarization that characterize the C-type inactivation process. On the contrary, the current amplitude of hKv1.5-T480A (**a**) and Shaker-T442A (**d**) gradually increased upon prolonged depolarization. Panel **b** and **e**, display the voltage dependence of channel inactivation for the WT channels (open circles) obtained by plotting the normalized current amplitude of the channel activating test pulse (I/Imax) as a function of the 5 s depolarizing voltage step. Stronger depolarizations induced after 5s approximately 60% of channel inactivation in both hKv1.5 (**b**) and Shaker (**e**). Plotting the normalized current amplitude of the activating test pulse for the 2nd-T-to-A mutations (filled

circles) resulted in the opposite behavior, the mutants channels did not inactivate and contradictorily displayed an increase of their current amplitude, **c.** and **f.** Activation (open circles) and inactivation (open triangles) time constants for the hKv1.5 (**e**) and Shaker (**f**) channels were obtained by fitting these two processes with an exponential function (note the semi-logarithmic axis). For comparison, the activation kinetics of the wild-type channel (from supplemental figure 1) are displayed with open circles. Upon 5s depolarization the hKv1.5-T480A activation (**a**) clearly contained two components and was best fitted with a double exponential function yielding a fast ($\tau_{fast}$, filled circles) and a slow ($\tau_{slow}$, filled triangles) time constant. Note that $\tau_{slow}$ in hKv1.5-T480A was comparable to the kinetics of wild-type inactivation and interestingly both are voltage-independent processes. The $\tau_{fast}$ kinetics of hKv1.5-T480A were similar to the activation time constants displayed in supplemental figure 1, which were obtained from analyzing the activation pulse protocols (i.e. current activations elicited with shorter depolarizing pulses). The Shaker-T442A mutant activation (**f**) was best approximated with a single exponential function yielding only the fast time component. (values represent mean ± se from 3 to 8 independent observations).

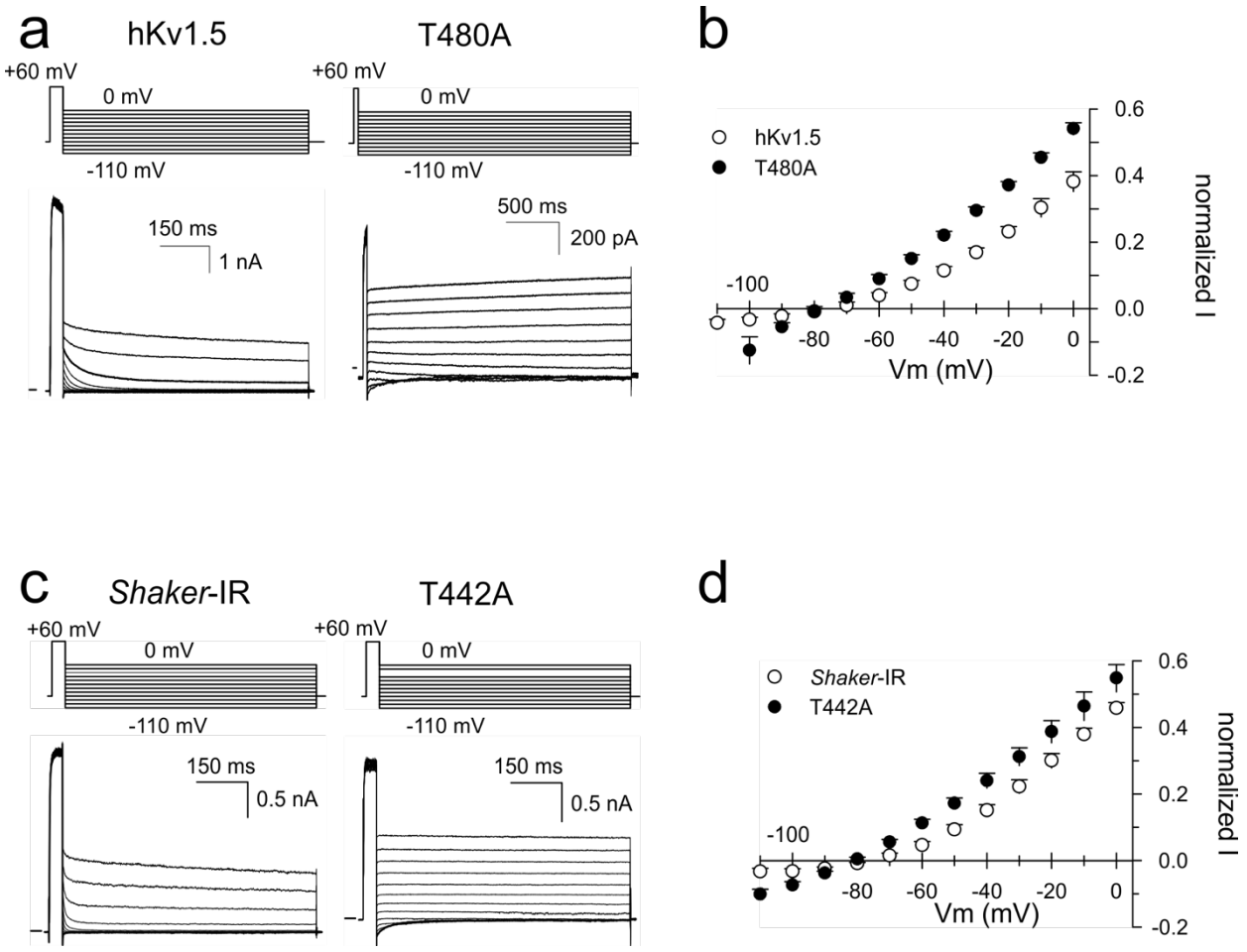


**Fig. S3.** 2nd-T-to-A mutations produced $K^+$ selective channels. Panels **a. and c.** show representative deactivating current recordings for hKv1.5 and its T480A mutation (**a**), and for *Shaker* and its T442A (**c**). Macroscopic current recordings were elicited with the pulse protocol shown at the top of the panel. The zero-current level is indicated by the horizontal bar at the start of the recordings. Panels **b and d** show current (I) versus voltage curves (IV curves) that were obtained by plotting the normalized amplitude of the deactivating current as a function of repolarizing potential. The IV curves of both the hKv1.5-T480A and Shaker-T442A mutant (filled circles) were comparable to the one of the wild-type channels (open circles). Wild-type and mutant channels displayed a similar reversal potential, which was used to calculate the channel´s ion selectivity (Table 1) in the following ionic conditions, 4 mM $K^+$ extracellular and 140 mM $K^+$ intracellular. A reversal potential of approximately -80 mV characterize the channel´s (wild-type and mutants) $K^+$ selectivity. (values represent mean ± se from 3 to 8 independent observations).

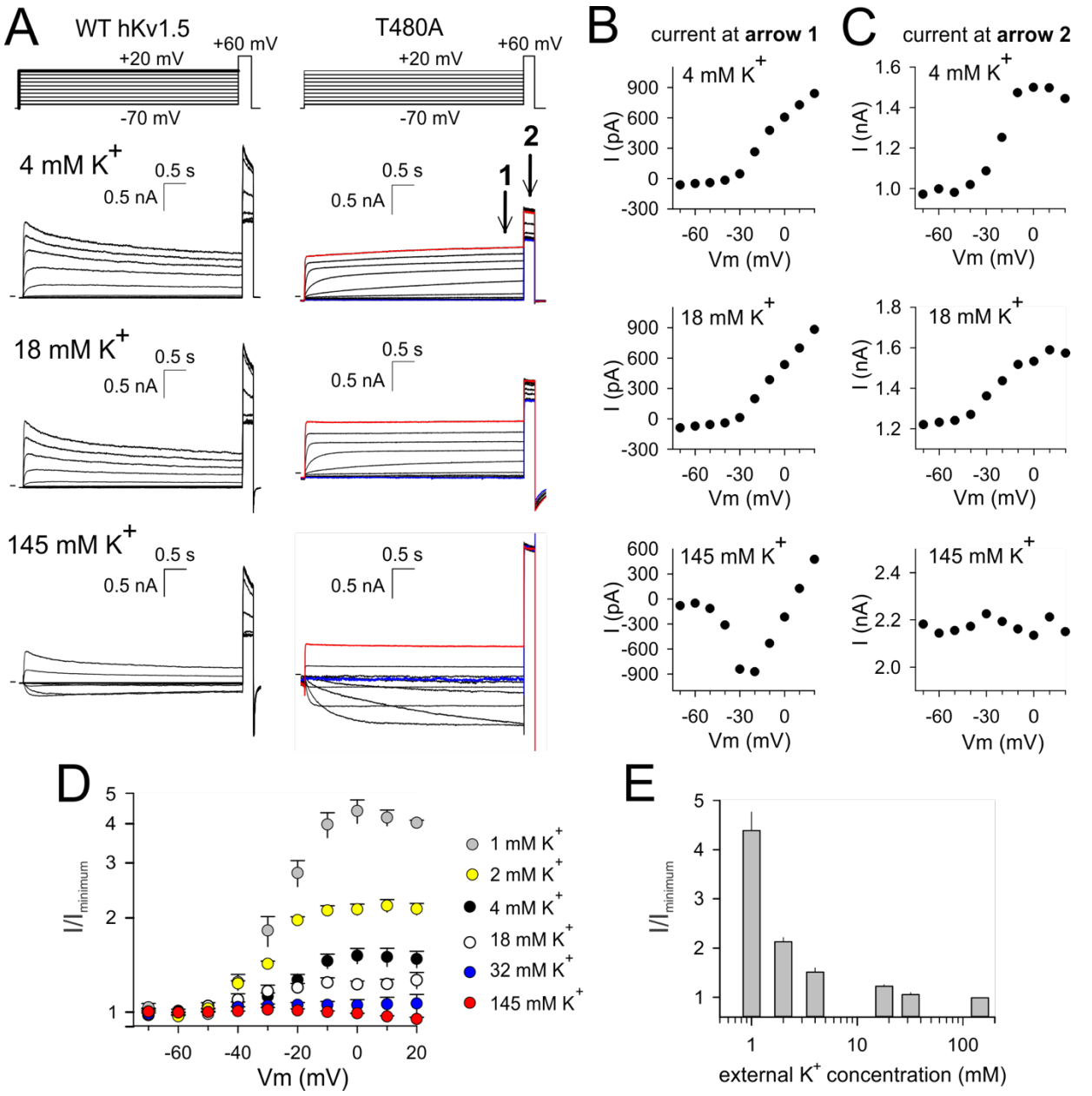


**Fig. S4.** Effect of the external $K^+$ concentration on the hKv1.5-T480A transition from an inactive to a conductive state**. a.** Representative macroscopic currents recordings of hKv1.5 (left) and the T480A mutant (right) measured in different external $K^+$ concentrations. Currents were elicited using the pulse protocol shown on top of panel **a**. The 5s conditioning depolarization steps were applied from -70 mV to + 20 mV with +10 mV increments and an inter-pulse duration of 1 minute at -80 mV. Before stepping down to a holding potential of -80 mV, a +60 mV activating pulse was applied to assess the

number of conductive channels. Macroscopic current recordings (from top bottom to top) were obtained at 4, 18 and 145 mM $K^+$ external $K^+$ concentration. The horizontal bar at the start of the recordings indicates the zero-current level. Increasing the external $K^+$ concentration lowers the $K^+$ chemical gradient resulting in the reduction of the current amplitude displayed by hKv1.5 channels at + 60 mV. Interestingly, the T480A mutant behaves opposite and the current amplitude at +60 mV get larger as the extracellular $K^+$ concentration is increased. In each set of macroscopic current recordings, the trace elicited upon a 5s pulse at -70 mV is colored blue and the one at +20 mV is displayed in red. In the wild type channels, a prolonged depolarization (e.g. to +20 mV) induces C-type inactivation, which reduces the number of conductive channels hence decreasing the current amplitude of the +60 mV test pulse. In contrast, prolonged depolarizations recruit the T480A channels to their conductive state and increases the current amplitude at +60 mV. Note that this increase was not observed at 145 mM external $K^+$ concentrations. **b.** Current versus voltage curves (IV curves) of the T480A mutant were obtained from the recordings displayed in panel **a**. by plotting the isochronal current amplitude at the end of the 5s depolarization pulse as a function of applied voltage (the point of measurement is indicated in panel **a.** by **arrow 1**). The IV curves show that the threshold of activation was not affected by the gradual increase of the external $K^+$ concentration. **c.** IV curves of the T480A mutant were obtained by plotting the current amplitude during the +60 mV activating pulse (**arrow 2** in panel **a**). These IV curves showed that the increase in T480A current amplitude, upon prolonged depolarizations, was smaller in high external $K^+$ concentration, when compare to the IV curve in 4 mM external $K^+$ concentration. However, the T480A total current amplitude was larger at 145 mM external $K^+$ concentration. This experimental result suggests that in high external $K^+$ concentration most of the T480A channels were fully conductive at the start of the depolarization pulse and there was no need of a 5s long depolarization to trigger interconversion from the non-conductive to the conductive conformation as seen in 4 mM external $K^+$. **d**. The normalized increase in current amplitude ($I/I_{minimum}$) during the +60 mV test pulse as a function of the 5s conditioning depolarization at different external $K^+$ concentrations. The increase in the current amplitude was most noticeable at low external $K^+$ concentrations, e.g. in 1 mM (gray symbols), 2 mM (yellow symbols) and 4 mM (black

symbols), respectively. Increasing the external $K^+$ concentration above 18 mM (white symbols) reduces the magnitude of the current amplitude increase and at 145 mM $K^+$ (red symbols) the increase was virtually absent. However, the total current amplitude at + 60 mV was larger at 145 mM external $K^+$ concentration (see panel **a** and **b**). **e**. Plot shows the normalized increase in current during a 5s depolarization pulse to 0 mV as a function of external $K^+$ concentration. (values represent mean ± se from 3 to 8 independent observations).

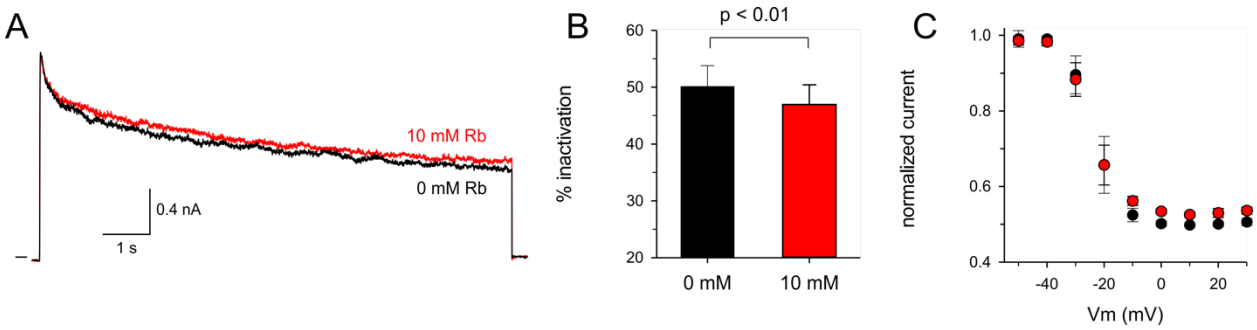


**Fig. S5.** External Rubidium slows inactivation in the WT-hKv1.5. **a**) Representative current recording of WT-hKv1.5 elicited with a 10 second depolarization to +50 mV (holding potential was -80 mV). Black trace was recorded in standard extracellular solution and the red trace subsequently in extracellular solution with 10 mM Rubidium. K+ concentration was similar in both extracellular solutions. In the presence of extracellular rubidium, hKv1.5 exhibited a reduction in the rate of C-type inactivation. Composition of the standard extracellular solution is reported in the methods section. **b**) Percentage of current inactivation in WT hKv1.5 after 5 s depolarization to +50 mV determined in standard extracellular solution (black bar, 0 mM Rb) or in presence of 10 mM Rb (red bar). The percentage of inactivation was determined by normalizing the current amplitude after 5 s depolarization to the peak current amplitude yielding 50.1 ± 3.7 % and 46.9 ± 3.5 % inactivation for 0 mM and 10 mM Rb, respectively (n = 5). Although the effect of extracellular Rb on reducing inactivation was small, the reduced inactivation with $Rb^+$ was observed in each of the cells analyzed and it was statistical significant ($p < 0.01$ with a standard t-test calculated in Origin). **c**) Voltage-dependence of channel inactivation obtained from analyzing current recordings at different membrane potentials. The current amplitude of the test pulse to +60 mV was normalized to the maximum and plotted as a function of the 5 s conditioning pre-pulse potential. Note that the voltage dependence of inactivation was in control conditions (black symbols) and in presence of 10 mM Rb (red symbols) similar (n = 5).

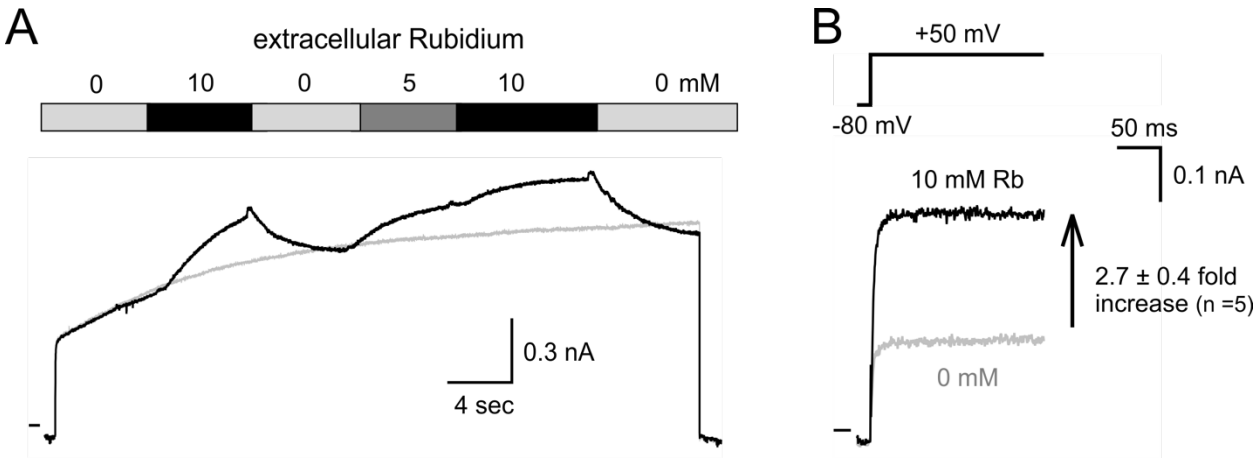


**Fig. S6.** External $Rb^+$ recruits hKv1.5-T480A channels to their conducting states. **a**) Using a pressurized fast perfusion system, the external solution was changed during a prolonged depolarization to +50 mV. Elevating the external $Rb^+$ concentration from 5 to 10 mM ($K^+$ concentration remained the same) increased T480A current amplitude gradually. Switching back to 0 mM $Rb^+$ (standard extracellular solution) resulted accordingly in a decrease of current amplitude. Gray current trace was recorded afterwards in standard extracellular solution (0 mM $Rb^+$) serving as a control. In agreement with the observation that $Rb^+$ reduced inactivation in WT hKv1.5, the recovery of hKv1.5-T480A channels to their conducting state was potentiated by $Rb^+$ as if they recovered from inactivation. **b**) Representative steady-state current activations at +50 mV in standard 0 mM $Rb^+$ extracellular solution (gray trace) and in 10 mM $Rb^+$ extracellular solution (black trace). In presence of 10 mM $Rb^+$ the current increased on average a 2.7-fold (n = 5).

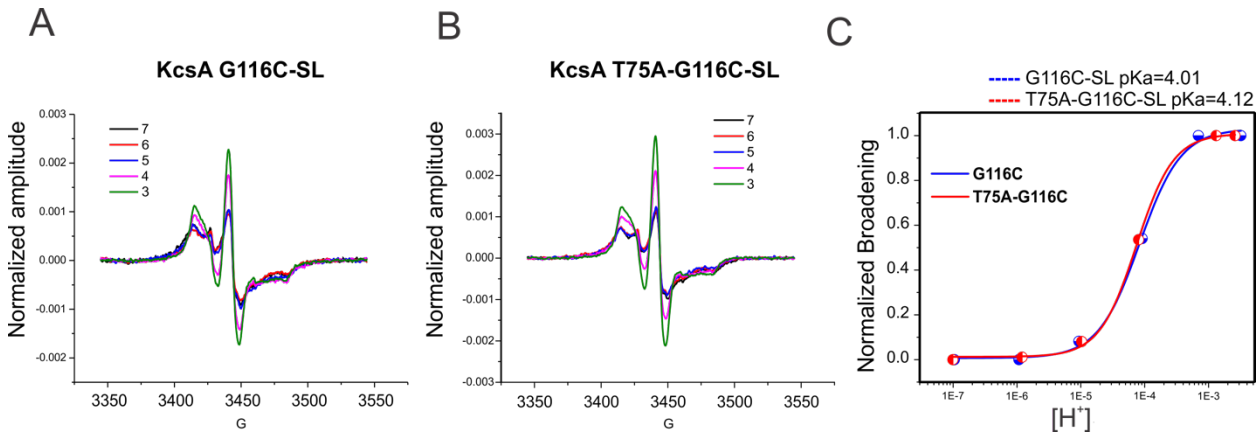


**Fig. S7.** Tracking the conformational changes at the KcsA-T75A's activation gate reveals a normal gating process. Continuous-wave electron paramagnetic resonance spectroscopy (CW-EPRs) measurements of a nitroxide group attached at KcsA's activation gate (G116C) for the wild-type **a.** and T75A mutant **b.** displayed characteristic pH-dependent line shape changes of the CW-EPR spectra. **c**. The pKa for activation of wild type KcsA is ~4.3±0.1. KcsA-T75A mutant channel exhibited almost identical pH-dependent conformational changes at its activation gate. The activation pKa for the T75A mutant measured in this condition was ~4.1±0.1 (values represent mean ± sd of 3 independent experimental observations)

**Reference**


1. Hoshi T, Zagotta WN, & Aldrich RW (1990) Biophysical and molecular mechanisms of Shaker potassium channel inactivation. *Science* 250(4980):533-538.
2. Boussif O*, et al.* (1995) A versatile vector for gene and oligonucleotide transfer into cells in culture and in vivo: polyethylenimine. *Proceedings of the National Academy of Sciences of the United States of America* 92(16):7297-7301.
3. Cortes DM & Perozo E (1997) Structural dynamics of the Streptomyces lividans K+ channel (SKC1): oligomeric stoichiometry and stability. *Biochemistry* 36(33):10343-10352.
4. Cuello LG, Cortes DM, & Perozo E (2017) The gating cycle of a K+ channel at atomic resolution. *eLife* 6.
5. Tilegenova C, Vemulapally S, Cortes DM, & Cuello LG (2016) An improved method for the cost-effective expression and purification of large quantities of KcsA. *Protein Expr Purif* 127:53-60.
6. Cortes DM, Cuello LG, & Perozo E (2001) Molecular architecture of full-length KcsA: role of cytoplasmic domains in ion permeation and activation gating. *The Journal of general physiology* 117(2):165-180.
7. **Otwinowski** Z & **Minor W** (1997) Macromolecular Crystallography, part A,. *Methods in Enzymology* 276:307-326.

8. Zhou M, Morais-Cabral JH, Mann S, & MacKinnon R (2001) Potassium channel receptor site for the inactivation gate and quaternary amine inhibitors. *Nature* 411(6838):657-661.
9. Emsley P & Cowtan K (2004) Coot: model-building tools for molecular graphics. *Acta Crystallogr D Biol Crystallogr* 60(Pt 12 Pt 1):2126-2132.
10. Adams PD*, et al.* (2010) PHENIX: a comprehensive Python-based system for macromolecular structure solution. *Acta Crystallogr D Biol Crystallogr* 66(Pt 2):213-221.